



# Segmentation of Pulmonary Nodules in CT Images Using the Sliding Band Filter

Joana Rocha<sup>1,2(✉)</sup>, António Cunha<sup>2,3</sup>, and Ana Maria Mendonça<sup>1,2</sup>

<sup>1</sup> Faculdade de Engenharia, Universidade do Porto,  
FEUP Campus, Dr. Roberto Frias, 4200-465 Porto, Portugal  
joana866rocha@gmail.com

<sup>2</sup> INESC TEC – INESC Technology and Science,  
FEUP Campus, Dr. Roberto Frias, 4200-465 Porto, Portugal

<sup>3</sup> Universidade de Trás-os-Montes e Alto Douro,  
Quinta de Prados, 5001-801 Vila Real, Portugal

**Abstract.** This paper proposes a conventional approach for pulmonary nodule segmentation, that uses the Sliding Band Filter to estimate the center of the nodule, and consequently the filter's support points, matching the initial border coordinates. This preliminary segmentation is then refined to try to include mainly the nodular area, and no other regions (e.g. vessels and pleural wall). The algorithm was tested on 2653 nodules from the LIDC database and achieved a Dice score of 0.663, yielding similar results to the ground truth reference, and thus being a promising tool to promote early lung cancer screening and improve nodule characterization.

**Keywords:** Lung · Nodule · Segmentation · Sliding band filter

## 1 Introduction

Pulmonary nodules can be associated with several diseases, but a recurrent diagnosis is lung cancer, which is the main cause of cancer death in men and the second cause in women worldwide [1]. For this reason, providing an early detection and diagnosis to the patient is crucial, considering that any delay in cancer detection might result in lack of treatment efficacy. The advances of technology and imaging techniques such as computed tomography (CT) have improved nodule identification and monitoring. In a CAD system, segmentation is the process of differentiating the nodule from other structures. However, this task is quite complex considering the heterogeneity of the size, texture, position, and shape of the nodules, and the fact that their intensity can vary within the borders. Data imbalance also poses a challenge, as in a CT scan less than 5% of the voxels belong to these lesions.

In biomedical image analysis, early methods (generally described as conventional) consisted of following a sequence of image processing steps (e.g. edge/line detectors, region growing) and mathematical models [2]. Afterwards, the idea of extracting features and feeding them to a statistical classifier made supervised

techniques become a trend. More recently, the trend is to use Deep Learning to develop models that are able to interpret what features better represent the data, but these require a large amount of annotated data, and have large computational cost. Among other conventional techniques, lesion detection and segmentation often imply the use of filters; e.g. the Sliding Band Filter can be used to develop an automated method for optic disc segmentation [4] and cell segmentation [5]. Such filter also proved to perform better than other local convergence index filters in pulmonary nodule detection [3]. This work aims to go further and precisely segment pulmonary nodules by implementing a conventional approach based on the Sliding Band Filter (SBF).

## 2 Local Convergence Filters and the Sliding Band Filter

Local Convergence Filters (LCFs) estimate the convergence degree,  $C$ , of the gradient vectors within a support region  $R$ , toward a central pixel of interest  $P(x, y)$ , assuming that the studied object has a convex shape and limited size range. LCFs aim to maximize the convergence index at each image point, which is calculated minding the orientation angle  $\theta_i(k, l)$  of the gradient vector at point  $(k, l)$  with respect to the line with direction  $i$  that connects  $(k, l)$  to  $P$ . The overall convergence is obtained by averaging the individual convergences at all  $M$  points in  $R$ , as written in Eq. 1, taken from [4].

$$C(x, y) = \frac{1}{M} \sum_{(k, l) \in R} \cos \theta_i(k, l) \quad (1)$$

LCFs perform better than other filters because they are not influenced by gradient magnitude, nor by the contrast with the surrounding structures. Being a member of the LCFs, the SBF also outputs a measure which estimates the degree of convergence of the gradient vectors. However, the position of the support region, which is a band of fixed width, is adapted according to the direction and the gradient orientation. The SBF studies the convergence along that band, ignoring the gradient's behaviour at the center of the object, which is considered irrelevant for shape estimation. Such feature makes this filter more versatile when it comes to detecting different shapes, even when they are not perfectly round, because the support region can be molded.

The SBF searches each one of the  $N$  radial directions leading out of  $P$  for the position of the band of fixed width  $d$  that maximizes the convergence degree. The search is done within a radial length that varies from a minimum ( $Rmin$ ) to a maximum ( $Rmax$ ) values, and so the filter's response is given by Eq. 2, where  $\theta_{i,m}$  represents the angle of the gradient vector at the point  $m$  pixels away from  $P$  in direction  $i$  [4]. The coordinates of the band's support points ( $X(\theta_i), Y(\theta_i)$ ) are obtained using Eq. 3, assuming that the center of the object is  $(x_c, y_c)$  [6].

$$SBF(x, y) = \frac{1}{N} \sum_{i=0}^{N-1} \max_{Rmin \leq r \leq Rmax} \left[ \frac{1}{d} \sum_{m=r-\frac{d}{2}}^{r+\frac{d}{2}} \cos \theta_{i,m} \right] \quad (2)$$

$$\begin{cases} X(\theta_i) = x_c + \underset{Rmin \leq r \leq Rmax}{argmax} \left[ \frac{1}{r} \sum_{m=r-\frac{d}{2}}^{r+\frac{d}{2}} \cos\theta_{i,m} \right] \times \cos(\theta_i) \\ Y(\theta_i) = y_c + \underset{Rmin \leq r \leq Rmax}{argmax} \left[ \frac{1}{r} \sum_{m=r-\frac{d}{2}}^{r+\frac{d}{2}} \cos\theta_{i,m} \right] \times \sin(\theta_i) \end{cases} \quad (3)$$

### 3 Methodology

The following algorithm was implemented on already detected nodules. For each nodule, the 3D volume around its center was split into three anatomical planes (sagittal, axial, and coronal), resulting in three  $80 \times 80$  pixel images per nodule. For clarity and brevity reasons, the method will be explained for a single plane, in Fig. 1a. The SBF is first applied to get a better estimation of the nodule's center coordinates. Considering most nodules have an overall uniform intensity, the nodules' images were processed by truncating any intensities much higher and lower than the nodule's. To do so, the nodule's average intensity was determined by calculating the mean of a matrix centered in the image. These steps result in a truncated mask, where there is already a very primitive segmentation (Fig. 1b) involving a low computational cost, which now needs substantial refinement.

The SBF takes the original nodule image, as well as the truncated nodule mask, and calculates its response in each pixel around the center of the image. The estimated nodule's center corresponds to the pixel which maximizes the response of the filter. With those coordinates, the SBF then evaluates the corresponding set of support points, returning the  $N$  border coordinates marked in Fig. 1c with yellow. To ensure the SBF is as precise as possible, a condition was added to force the cosine of the gradient vector's orientation angle to be null when the pixel which is being evaluated in a certain direction is black in the truncated mask. Ideally, this keeps the SBF from including in the segmentation non-nodular regions within the  $Rmin$  and  $Rmax$  limits. An outlier attenuation/removal step was implemented, minding the distance between consecutive border coordinates, and afterwards a binary mask with the initial SBF segmentation is created. To further refine the segmentation and specifically select the nodular area, only the intersection of the SBF segmentation mask and the truncated nodule mask is considered, thus eliminating unwanted regions. Any cavities within the intersected binary masks are filled, and the result is displayed in Fig. 1e. By labeling all the different regions present in the intersected masks, which are identified by their connected components, it is possible to eliminate any region that has no connection to the nodule. This can be done by eliminating from the mask all regions that do not encompass the center of the image, as the nodule is always centered. After this step, the final segmentation mask is achieved, as exemplified in Fig. 1d.

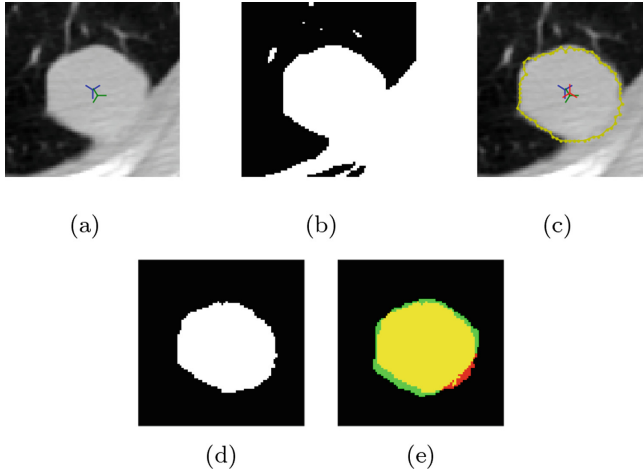


**Fig. 1.** Exemplification of the methodology steps, where the blue mark is the center of the image, the green mark is the ground truth center of the nodule, and the red mark is the estimated center of the nodule.

## 4 Results

The method was evaluated on 2653 nodules, using as ground truth the segmentation masks from the LIDC database, which is publicly available and consists of lung cancer screening thoracic CT scans from 1010 patients. These results were obtained with the SBF parameter values  $N = 64$ ,  $d = 7$ ,  $Rmin = 1$ , and  $Rmax = 25$ , which were established empirically to maximize the algorithm's performance. The method achieved a Dice score of 0.663, while having Precision and Recall values of 0.710 and 0.732, respectively. Figure 1e compares the achieved segmentation with the ground truth, in which the green pixels belong exclusively to the ground truth mask, the red pixels belong exclusively to the achieved result using the proposed method, and the yellow pixels belong to both - meaning that the yellow pixels mark the correct predictions made by the algorithm. The proposed conventional approach exhibits a highly satisfactory performance when dealing with well-circumscribed solid nodules. The nodules that have a pleural tail generally have the thin structure ignored by the algorithm, which does not include it in the segmentation mask, while the specialists consider the tail as part of the nodule. In spite of vascularized nodules entailing an inherent difficulty when it comes to distinguishing the nodule from the attached vessels, the SBF based approach is frequently able to separate them and create a mask which does not include the non-nodular structures. The algorithm's performance is also satisfying when dealing with nodules whose intensities vary within their border (e.g. calcific and cavitary nodules), as it is able to ignore the cavities/calcific regions during the segmentation process. The main flaws of the algorithm appear when dealing with juxtapleural nodules, since it often does not know where the nodule ends and the pleura begins, thus only being able to

estimate the boundary to some extent. Overall, the less satisfying results are mainly due to the unexpected shape of the nodule, or because the nodule does not have a clear margin (e.g. non-solid nodules/ground glass opacities).

## 5 Conclusion

The segmentation of pulmonary nodules contributes to their characterization, which makes it a key to assess the patient's health state. This way, a segmentation step implemented within a CAD system can help the physician establish a more accurate diagnosis. However, the automation of such task is hampered by the diversity of nodule shape, size, position, lighting, texture, etc. The proposed conventional approach deals with these challenges by implementing the Sliding Band Filter to find the coordinates of the borders, and achieves a Jaccard score of 0.990 when tested with the LIDC database. This is a robust method for different nodule types, particularly well-circumscribed, solid and/or vascularized nodules. Its performance is impaired by juxtapleural lesions, and irregular shaped/non-solid nodules, and so future work includes the refinement of this method to deal with these particular challenges. Finally, it is possible to conclude this is a promising segmentation method, thus contributing to the clinically relevant characterization of pulmonary nodules.

**Conflict of Interest.** The authors declare no conflict of interest. This work is financed by National Funds through the Portuguese funding agency, FCT - Fundação para a Ciência e a Tecnologia within project: UID/EEA/50014/2019.

## References

1. Torre, L.A., Siegel, R.L., Jemal, A.: Lung cancer statistics. In: Lung Cancer and Personalized Medicine, pp. 1–19. Springer, Cham (2016). [https://doi.org/10.1007/978-3-319-24223-1\\_1](https://doi.org/10.1007/978-3-319-24223-1_1)
2. Litjens, G., Kooi, T., Bejnordi, B.E., Setio, A.A.A., Ciompi, F., Ghafoorian, M., Sánchez, C.I.: A survey on deep learning in medical image analysis. *Med. Image Anal.* **42**, 60–88 (2017). <https://doi.org/10.1016/j.media.2017.07.005>
3. Pereira, C.S., Mendonça, A.M., Campilho, A.: Evaluation of contrast enhancement filters for lung nodule detection. In: International Conference Image Analysis and Recognition, pp. 878–888. Springer, Heidelberg, August 2007. [https://doi.org/10.1007/978-3-540-74260-9\\_78](https://doi.org/10.1007/978-3-540-74260-9_78)
4. Dashtbozorg, B., Mendonça, A.M., Campilho, A.: Optic disc segmentation using the sliding band filter. *Comput. Biol. Med.* **56**, 1–12 (2015). <https://doi.org/10.1016/j.combiomed.2014.10.009>
5. Quelhas, P., Marcuzzo, M., Mendonça, A.M., Campilho, A.: Cell nuclei and cytoplasm joint segmentation using the sliding band filter. *IEEE Trans. Med. Imaging* **29**(8), 1463–1473 (2010). <https://doi.org/10.1109/TMI.2010.2048253>
6. Shakibapour, E., Cunha, A., Aresta, G., Mendonça, A.M., Campilho, A.: An unsupervised metaheuristic search approach for segmentation and volume measurement of pulmonary nodules in lung CT scans. *Expert Syst. Appl.* **119**, 415–428 (2019). <https://doi.org/10.1016/j.eswa.2018.11.010>